Journal of *Marine Science and Engineering*

MDPI

Article

Ocean Warming Amplifies the Effects of Ocean Acidification on Skeletal Mineralogy and Microstructure in the Asterinid Starfish *Aquilonastra yairi*

Munawar Khalil [1,2,3,*], Steve S. Doo [1,4], Marleen Stuhr [1] and Hildegard Westphal [1,2,4]

[1] Leibniz Centre for Tropical Marine Research (ZMT), 28359 Bremen, Germany; steve.doo@leibniz-zmt.de (S.S.D.); marleen.stuhr@leibniz-zmt.de (M.S.); hildegard.westphal@kaust.edu.sa (H.W.)
[2] Faculty of Geosciences, University of Bremen, 28359 Bremen, Germany
[3] Department of Marine Science, Faculty of Agriculture, Universitas Malikussaleh, Reuleut Main Campus, Aceh 24355, Indonesia
[4] Physical Science and Engineering (PSE), Red Sea Research Center (RSRC), King Abdullah University of Science and Technology (KAUST), Thuwal 23955-6900, Saudi Arabia
* Correspondence: munawar.khalil@leibniz-zmt.de

Abstract: Ocean acidification and ocean warming compromise the capacity of calcifying marine organisms to generate and maintain their skeletons. While many marine calcifying organisms precipitate low-Mg calcite or aragonite, the skeleton of echinoderms consists of more soluble Mg-calcite. To assess the impact of exposure to elevated temperature and increased pCO_2 on the skeleton of echinoderms, in particular the mineralogy and microstructure, the starfish *Aquilonastra yairi* (Echinodermata: Asteroidea) was exposed for 90 days to simulated ocean warming (27 °C and 32 °C) and ocean acidification (455 µatm, 1052 µatm, 2066 µatm) conditions. The results indicate that temperature is the major factor controlling the skeletal Mg (Mg/Ca ratio and Mg_{norm} ratio), but not for skeletal Sr (Sr/Ca ratio and Sr_{norm} ratio) and skeletal Ca (Ca_{norm} ratio) in *A. yairi*. Nevertheless, inter-individual variability in skeletal Sr and Ca ratios increased with higher temperature. Elevated pCO_2 did not induce any statistically significant element alterations of the skeleton in all treatments over the incubation time, but increased pCO_2 concentrations might possess an indirect effect on skeletal mineral ratio alteration. The influence of increased pCO_2 was more relevant than that of increased temperature on skeletal microstructures. pCO_2 as a sole stressor caused alterations on stereom structure and degradation on the skeletal structure of *A. yairi*, whereas temperature did not; however, skeletons exposed to elevated pCO_2 and high temperature show a strongly altered skeleton structure compared to ambient temperature. These results indicate that ocean warming might exacerbate the skeletal maintaining mechanisms of the starfish in a high pCO_2 environment and could potentially modify the morphology and functions of the starfish skeleton.

Keywords: ocean acidification; ocean warming; echinoderm; starfish; mineralogy; skeleton; biomineralization

Citation: Khalil, M.; Doo, S.S.; Stuhr, M.; Westphal, H. Ocean Warming Amplifies the Effects of Ocean Acidification on Skeletal Mineralogy and Microstructure in the Asterinid Starfish *Aquilonastra yairi*. *J. Mar. Sci. Eng.* **2022**, *10*, 1065. https://doi.org/10.3390/jmse10081065

Academic Editor: Markes E. Johnson

Received: 31 May 2022
Accepted: 1 July 2022
Published: 3 August 2022

1. Introduction

The oceans are estimated to take up ~31% of the CO_2 increase that is currently observed [1]. This is known to lead to lowered pH values of the seawater, resulting in a reduced carbonate saturation state (Ω), and changes in carbonate–bicarbonate ion balance, recognized as ocean acidification (OA) [2,3]. These changes in seawater chemistry lead to measurable reactions of marine species and ecosystems, and are known to have negative repercussions for many calcifying organisms [4–7], including certain scleractinian corals, bryozoans, molluscs, and echinoderms. Decreased carbonate ion concentration [CO_3^{2-}] can disrupt the physiologically regulated biomineralization mechanism that generates, preserves and maintains calcium carbonate ($CaCO_3$) structures, e.g., exoskeleton, test,

spine, tube feet, teeth, pedicellariae and spicules [4,8–10]. This mechanism involves mineral formation, characteristics, morphogenesis, and organic molecules [9,11–13]. This is particularly the case for organisms precipitating a skeleton composed of high Mg-calcite (HMC) i.e., with a significant concentration of magnesium carbonate ($MgCO_3$) in the carbonate (>4 mol% $MgCO_3$) [14,15]. HMC is the most soluble of the polymorphs of crystalline $CaCO_3$ and is thermodynamically metastable [14,16]. Furthermore, previous studies have shown that OA significantly affects the size and weight of shells or skeletons of many marine calcifiers [17–19]. In contrast, some calcifiers, mainly photosynthesizing or photosymbiotic ones, including some corals and algae, show positive responses in calcification and growth values as they benefit from increased CO_2 concentrations by an enhanced photosynthesis rate, which provides additional potential energy for the calcification process [20].

At the same time, seawater temperature (ocean warming, OW) influences the ecophysiology of marine organisms [21], skeletal mineralogy [11,14,22–27], growth rate [28], and mineral growth control mechanisms [29]. Previous studies have found inconsistent reactions to increased temperature exposure, ranging from no effect to significant changes in skeletal mineralogy. For example, the skeletal Mg/Ca ratios of the scleractinian coral *Acropora* sp. [30], the sea urchin *Paracentrotus lividus* [25], the foraminifera *Planoglabratella operculari*, *Quinqueloculina yabei* [31] and *Ammonia tepida* [32] increase with temperature; conversely, the skeletal Mg/Ca ratios of the sea urchin *Lytechinus variegatus* was significantly lower in individuals kept at high temperature (~30 °C) compared to the ambient temperature (~26 °C) [26]. Skeletal Sr/Ca ratios decreases with increasing temperature in the scleractinian coral *Acropora* sp. [30,33], Sr/Ca ratios increases with increasing temperature in the foraminifera *A. tepida* [32] or Globigerinoides ruber [34], and is not significantly affected by temperature in the foraminifera *Trifarina angulosa* [35]. However, the effects of temperature on skeletal mineralogy and structure are still largely unclear and are likely influenced by phylogenetic factors, growth rate [22,23,36], latitude [24], biological 'vital effects' [37], and stage or species-specific differences [38].

The effects of combined OA and OW on marine calcifiers organisms are thought to be additive, antagonistic, or synergistic [39]. Previous meta-studies observed complex responses of calcifying marine organisms to combined OW and OA that vary from a significant negative effect to no effect on the organism [40]. Moreover, there is a trend toward enhanced sensitivity (i.e., the capability to sense and respond to environmental alterations) of biomineralization, growth, survival, and life stages development to OA in corals, echinoderm, and molluscs when being concurrently exposed to elevated temperatures [41]. Besides, there is growing evidence that elevated temperatures can exacerbate microstructure disruption caused by elevated pCO_2 in ectotherm species, e.g., in some molluscs such as the giant clam *Tridacna maxima* [42] and the mussel *Mytilus edulis* [43,44], and echinoderms such as the sea urchin *Tripneustes gratilla* [45]. However, these synergistic effects of OA and OW seem to be complex, and the magnitude of effect sizes and organism response varies between taxa groups, trophic level, habitat and life stages [40,41,46].

Echinoderms comprise a wide variety of taxa, with a complex calcium carbonate biomineralization. Their skeleton is formed within the syncytium by progressive crystallization of a transient amorphous calcium carbonate phase (ACC) [47], through a biologically controlled intracellular mechanism within vesicles or vacuoles formed by fused cell membranes inside cells [11,22,48]. The echinoderm endoskeleton is composed of a complex three-dimensional porous microstructure (stereom) with connecting trabeculae (i.e., mesh-like interconnecting matrix rod of calcite skeleton) [11], which are composed of 99.8–99.9% weight/weight (w/w) HMC with Sr as the primary trace element [49,50], and the other 0.1–0.2% (w/w) of the skeleton being organic components consisting of proteins and glycoproteins, called the intrastereomic organic matrix (IOM) [51,52]. The IOM has critical functions in the biomineralization process during the transient ACC phase by stabilizing the skeleton, controlling mineral incorporation into the skeleton, and controlling the nucleation and morphology of the skeletal crystals [53,54]. The trace element concentration of biogenic $CaCO_3$ is affected by biological factors, e.g., phylogeny, life stage, food supply,

as well as by physical-chemical factors, e.g., temperature, salinity, seawater carbonate chemistry, concentration of Mg^{2+} and Ca^{2+} ions in the seawater, light, and hydrostatic pressure [14,27,37,49,55,56]. Seawater chemistry influences the mineralogy of the echinoderm skeleton by changing the physiological cost of sustaining the biological control of intracellular chemistry [57]. For echinoderms with their skeletons being composed of HMC ($MgCO_3$ between 2.5% and 39% [8]), their skeletons become more soluble under OA conditions [16,50,58,59].

To gain a better understanding of the effects of combined OA and OW on biomineralization, systematic comparative studies across a phylogenetically diverse spectrum of taxa are needed [57]. The present study contributes to this goal by investigating the mineral composition and skeleton microstructure of *Aquilonastra yairi* (phylum Echinodermata, class Asteroidea, family Asterinidae) under controlled OA and OW conditions. This asterinid starfish thrives in the marine intertidal and coral reefs of the Red Sea and the Mediterranean Sea, where it lives in crevices and beneath corals or rocks [60]. It has an important ecological function as a grazer of marine algae, bacterial mats, detritus, and other fragments of food [61]. Previous studies have indicated deleterious effects of combined OA and OW on the physiological performances of asterinid starfish [62–65], while the effects of each stressor and their potential synergetic effects on skeletal mineral ratio and microstructure are currently still poorly understood.

2. Materials and Methods

2.1. Experimental Design and Control of Seawater Chemistry

In this study, starfish *A. yairi* was used as a model organism to investigate the combined effects of OW and OA. A total of 342 specimens of *A. yairi* (size 3–11 mm) from the cultivated stock of the MAREE (Marine Experimental Ecology facility) of ZMT, Bremen, Germany, were studied in the present experiment. Following acclimation procedures (see electronic Supplementary Materials), the starfish were cultured for 90-days in six different treatments, namely at two different temperatures (ambient temperature: 27 °C, and high temperature: 32 °C) crossed with three levels of pCO_2 (low pCO_2: 455 µatm, medium pCO_2: 1052 µatm, and high pCO_2: 2066 µatm). All six treatments were replicated in three aquaria (electronic Supplementary Materials Figure S1).

Target temperature and pCO_2 levels were ramped up gradually over the first ten days to avoid physiological shock. Then the temperature (mean ± SE) in the treatment tanks was maintained at 27 ± 0.05 °C and 32 ± 0.08 °C, respectively, using a closed circle heating system (Heaters Titanium Tube 600 W, Schego Schemel & Goetz, Offenbach, Germany), controlled with a programmable thermostat. The mixture of the gas bubbled into the seawater in the bottom storage compartment sump was reached by blending compressed CO_2-free air and compressed CO_2 (pure CO_2 provided by Linde GmbH, Pullach, Germany) using electronic solenoid-valve mass-flow controllers (HTK Hamburg GmbH, Hamburg, Germany) in accordance with the standard operating procedure (SOP) for ocean CO_2 measurements [66]. Details of the seawater chemistry control and manipulation are provided in the electronic Supplementary Materials. The seawater parameters and carbonate chemistry for the experimental exposures are given in Table 1.

Table 1. Seawater chemistry values measured during a 90-day experimental period for *A. yairi* reared under two temperature levels (27 °C and 32 °C) crossed with three levels of pCO_2 (455 µatm, 1052 µatm, and 2066 µatm). A_T, total alkalinity; DIC, dissolved inorganic carbon; pCO_2, partial pressure of CO_2; [CO_3^{2-}], carbonate ion concentration; [HCO_3^-], bicarbonate ion concentration; [CO_2], dissolved CO_2; Ω_{Ca}, calcite saturation state; Ω_{Ar}, aragonite saturation state. Data are presented as mean values ± SE.

Treatment	Measured Parameters					
	Salinity (PSU)	Temperature (°C)	$pH_{(NBS\ scale)}$	$pH_{(total\ scale)}$	A_T (µmol/kg-SW)	DIC (µmol/kg-SW
27 °C: 455 µatm	34.56 ± 0.12	27.48 ± 0.06	8.13 ± 0.00	8.00 ± 0.00	2504.42 ± 15.33	2168.86 ± 15.23
27 °C: 1052 µatm	34.73 ± 0.06	27.23 ± 0.04	7.87 ± 0.01	7.74 ± 0.01	2514.45 ± 16.78	2340.99 ± 11.62
27 °C: 2066 µatm	34.75 ± 0.05	27.34 ± 0.03	7.60 ± 0.01	7.47 ± 0.01	2539.83 ± 38.86	2479.40 ± 36.58
32 °C: 455 µatm	34.65 ± 0.08	32.03 ± 0.05	8.13 ± 0.00	8.00 ± 0.00	2510.27 ± 47.18	2134.38 ± 38.40
32 °C: 1052 µatm	34.78 ± 0.05	32.10 ± 0.04	7.87 ± 0.00	7.74 ± 0.00	2532.19 ± 40.05	2325.20 ± 40.02
32 °C: 2066 µatm	34.76 ± 0.02	32.20 ± 0.08	7.60 ± 0.01	7.47 ± 0.01	2584.38 ± 41.93	2493.30 ± 37.87
Treatment	**Calculated Parameters**					
	pCO_2 (µatm)	[CO_3^{2-}] (µmol/kg-SW)	[HCO_3^-] (µmol/kg-SW)	[CO_2] (µmol/kg-SW)	Ω_{Ca}	Ω_{Ar}
27 °C: 455 µatm	456.13 ± 8.24	245.64 ± 2.52	1911.05 ± 14.94	12.17 ± 0.22	5.96 ± 0.06	3.96 ± 0.04
27 °C: 1052 µatm	1059.58 ± 32.04	138.12 ± 4.64	2178.74 ± 9.58	28.42 ± 0.86	3.35 ± 0.11	2.22 ± 0.07
27 °C: 2066 µatm	2075.40 ± 30.99	81.18 ± 2.35	2342.71 ± 34.29	55.51 ± 0.82	1.97 ± 0.06	1.31 ± 0.04
32 °C: 455 µatm	453.78 ± 6.51	273.82 ± 8.23	1849.66 ± 30.77	10.90 ± 0.16	6.71 ± 0.20	4.52 ± 0.14
32 °C: 1052 µatm	1045.15 ± 44.00	162.68 ± 4.67	2147.47 ± 38.59	25.05 ± 1.06	3.98 ± 0.11	2.69 ± 0.08
32 °C: 2066 µatm	2057.31 ± 74.42	99.46 ± 4.64	2344.63 ± 34.94	49.20 ± 1.78	2.44 ± 0.11	1.64 ± 0.08

2.2. Skeletal Mineral Composition Analysis

On days 45 and 90 of the experimental treatment, six specimens from each replicate tank (i.e., 36 in total on each of those days) were randomly collected and rinsed in Milli-Q (18.2 MΩ) water before drying for ~48 h at 40 °C. In preparation for trace element analysis, to remove organic material from the skeletal matrix, dried starfish were soaked in hydrogen peroxide (H_2O_2) [67–69] for 24 h and subsequently cleaned mechanically, i.e., residual organic material was removed by forceps, and further potential contaminations were removed with deionized water in an ultrasonic bath. Then, the sample material was manually ground using a mortar and pestle. The powdered samples were kept at room temperature in sealed vials until analysis.

The element concentration of Ca, Mg and Sr in the skeleton was determined with a Spectro CIROS Vision (SPECTRO Analytical Instruments GmbH, Kleve, Germany) inductively coupled plasma optical emission spectroscope (ICP-OES). The samples (weighing 0.02–0.1 mg) were digested with concentrated nitric acid (HNO_3) and H_2O_2 (high-purity of trace metal grade reagent). The solutions were then diluted to the acidity of 0.5 M HNO_3 with aliquots of 0.1 mL and weighed again. Instrument calibration solutions (Inorganic Ventures^{TM} 1000 ppm standard stock solution) were prepared using single-element standards in proportion to the *A. yairi* skeleton concentrations. Measurements of all starfish samples were done routinely against the international reference standard JLs^{-1}, a coral in-house working standard ($ZMT\text{-}CM_1$), and HNO_3 blanks. Mg and Sr mineral elements are reported as a ratio over calcium (Ca), i.e., Mg/Ca, and Sr/Ca and over total skeletal material, i.e., Ca_{norm}, Mg_{norm}, and Sr_{norm}, to account for minor organic material still present on or within the carbonate skeleton.

2.3. Analysis of the Skeleton Microstructure

One specimen from the 45-day and 90-day incubations from each treatment tank was randomly selected (n = 12), washed, and prepared for the SEM analysis. Each starfish was cut with dissecting scissors around the part of arms and cleaned of soft tissue. Organic material was dissolved using a 30% H_2O_2 solution buffered in NaOH (0.1 N) at room temperature for 24 h. Skeletons were then rinsed with distilled water repeatedly to

remove any remaining organic material and then air-dried for 48 h at room temperature. Skeleton plates were then mounted on a stub with carbon-based tape and gold-sputtered (Cressington Sputter Coater 108 auto, Cressington Scientific Instruments, Watford, UK) for 30 s. Secondary electron images (SE) were generated with a scanning electron microscope (SEM; Tescan Vega3 XMU, Brno-Kohoutovice, Czech Republic) to characterize the skeleton microstructure, using a beam voltage of 5 kV for a magnification of up to 3000×. All SEM micrographs were examined for any visible differences between treatments, including signs of dissolution, surface smoothness, the shape of stereom pores, and the shape of inner matrix aperture pores.

2.4. Statistical Analysis

Statistical analysis was performed using the software R, version 4.1.3 [70]. Normality of data distribution and homogeneity of variance was tested with the Shapiro–Wilk statistic W test ($\alpha = 0.05$) [71] and Levene's test ($\alpha = 0.05$) [72], respectively, and indicated that all data of skeletal mineral ratios were normally distributed and the homoscedasticity assumption for the data was equal. The effects of temperature, pCO_2, incubation time and their interactions on skeletal mineral element to calcium ratios (Mg/Ca and Sr/Ca) and skeletal mineral element to total skeletal material ratios (Ca_{norm}, Mg_{norm}, and Sr_{norm}) were examined using three-way analysis of variance (ANOVA), and Tukey HSD post hoc analyses were conducted using agricolae R-package 1.3-5 [73]. Temperature, pCO_2, and incubation time were fixed factors, while skeletal mineral ratios were used as response variables. All statistics were evaluated with a significance level of $\alpha = 0.05$.

3. Results

Over the duration of the experiment (90 days), the starfish mortality rate was low and only found in the high-temperature treatment. In general, the results indicate that elevated temperature and pCO_2 changed the skeletal mineral composition, whereas elevated pCO_2 affected skeletal microstructure in *A. yairi*.

3.1. Elemental Composition of Skeletal Carbonate

Overall, a relatively small range of Mg/Ca ratio values were observed across all our treatments (181.95–204.26 mmol/mol). The starfish had consistently higher Mg/Ca ratios in the 32 °C treatments (190.90 ± 1.41 mmol/mol, mean ± SE) than those held at 27 °C (187.59 ± 0.83 mmol/mol, mean ± SE) throughout all pCO_2 concentration levels. Both incubation time and temperature had a main effect on skeletal Mg/Ca ratio ($p = 0.049$ and $p = 0.033$, respectively; Table 2). Inter-individual variability in skeletal Mg/Ca ratios was substantially higher in starfish subjected to high temperatures (32 °C) compared to those exposed to ambient temperatures (27 °C) in all pCO_2 combined treatments (Figure 1A). No consistent pCO_2 effect as the sole factor was found, and the Mg/Ca ratio displayed the typical parabolic responses to pCO_2 (Figure 1A). Elevated pCO_2 as the sole stressor did not significantly affect skeletal Mg/Ca ratios ($p = 0.414$, Table 2). The interaction of temperature: pCO_2: incubation time on starfish skeletal Mg/Ca ratios was significant ($p = 0.014$, Table 2). However, Tukey's HSD post hoc analysis did not reveal any significant interactions in Mg/Ca ratios (Table 2 and electronic Supplementary Materials Table S1).

Table 2. Summary of three-way ANOVA results for the skeletal mineral ratios of *A. yairi* exposed to temperature (27 °C, 32 °C) crossed with elevated pCO_2 (455 µatm, 1052 µatm, 2066 µatm) treatments for 45 and 90 days incubation time. Tukey HSD post hoc tests were performed where ANOVA results indicated significant effects of one or several factors (incubation time, pCO_2, temperature) with *p*-values adjusted for multiple testing (p_{adj}). Bold terms indicate a significant difference ($p < 0.05$).

Skeletal Mineral Ratio	df	F	Pr (<F)	Post-Hoc Test Result
Mg/Ca ratio				
Incubation time	1	4.319	**0.049**	90 days > 45 days
pCO_2	2	0.915	0.414	
Temperature	1	5.144	**0.033**	32 °C > 27 °C
Incubation time: pCO_2	2	0.715	0.500	
Incubation time:temperature	1	0.039	0.845	
pCO_2: temperature	2	0.478	0.626	
Incubation time: pCO_2: temperature	2	5.143	**0.014**	n.s., electronic Supplementary Materials Table S1
Residuals	24			
Sr/Ca ratio				
Incubation time	1	9.027	**0.006**	90 days > 45 days
pCO_2	2	0.405	0.671	
Temperature	1	0.481	0.495	
Incubation time: pCO_2	2	1.794	0.188	
Incubation time: temperature	1	1.519	0.230	
pCO_2: temperature	2	2.016	0.155	
Incubation time: pCO_2: temperature	2	1.132	0.339	
Residuals	24			
Ca_{norm} ratio				
Incubation time	1	4.951	**0.036**	90 days > 45 days
pCO_2	2	1.242	0.307	
Temperature	1	0.043	0.838	
Incubation time: pCO_2	2	1.711	0.202	
Incubation time: temperature	1	0.59	0.450	
pCO_2: temperature	2	1.471	0.250	
Incubation time: pCO_2: temperature	2	1.65	0.213	
Residuals	24			
Mg_{norm} ratio				
Incubation time	1	24.523	**0.001**	90 days > 45 days
pCO_2	2	0.582	0.566	
Temperature	1	4.206	**0.051**	32 °C > 27 °C
Incubation time: pCO_2	2	0.616	0.548	
Incubation time: temperature	1	0.621	0.438	
pCO_2: temperature	2	0.609	0.552	
Incubation time: pCO_2: temperature	2	2.133	0.140	
Residuals	24			
Sr_{norm} ratio				
Incubation time	1	9.814	**0.005**	90 days > 45 days
pCO_2	2	0.500	0.613	
Temperature	1	0.156	0.696	
Incubation time: pCO_2	2	1.862	0.177	
Incubation time: temperature	1	1.405	0.248	
pCO_2: temperature	2	1.655	0.212	
Incubation time: pCO_2: temperature	2	0.707	0.503	
Residuals	24			

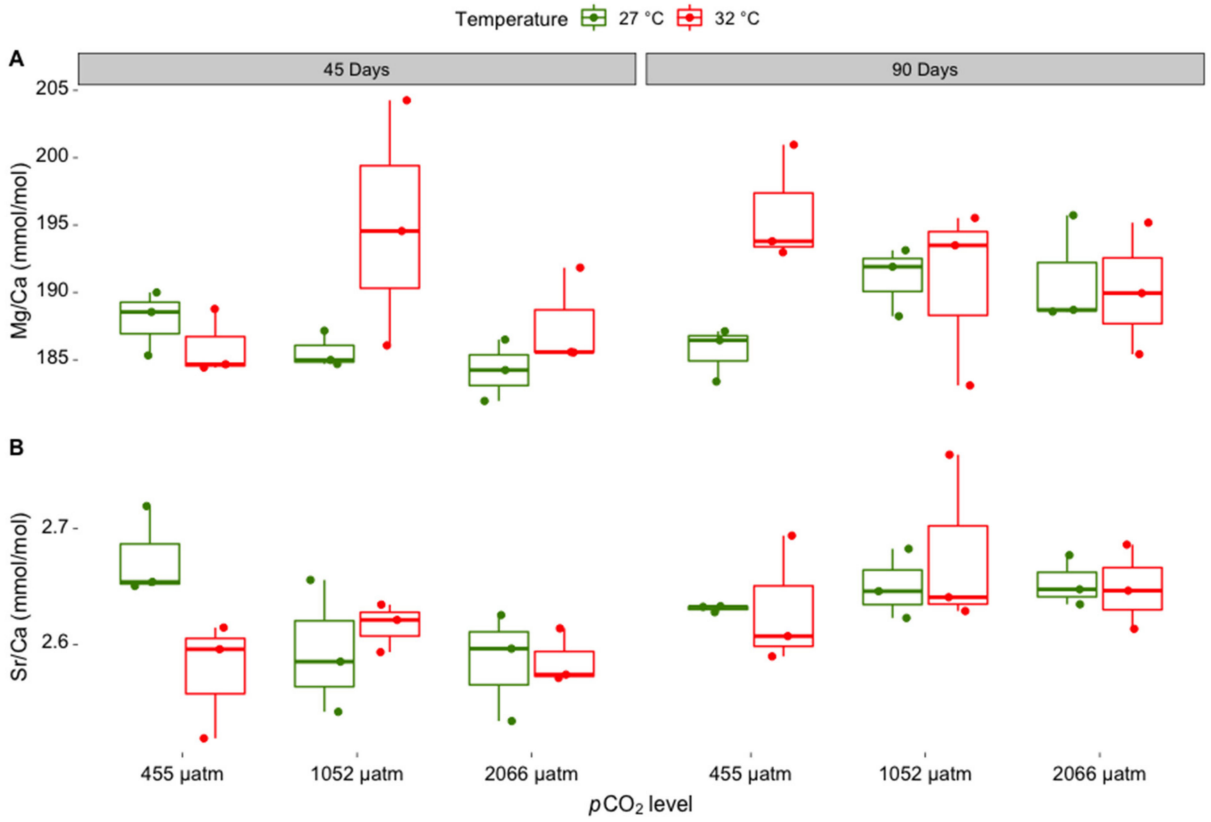

Figure 1. Changes in skeletal properties (**A**) Mg/Ca ratios (mmol/mol) and (**B**) Sr/Ca ratios (mmol/mol) of skeletal carbonate in *A. yairi* exposed to different temperatures (27 °C and 32 °C) crossed with different pCO_2 concentrations (455 µatm, 1052 µatm, and 2066 µatm) measured after 45 and 90 days of incubation (n = 36). Dots represent individual skeletal mineral values, displayed with jitter to avoid overlap.

Sr/Ca ratios ranged from 2.52 mmol/mol to 2.76 mmol/mol across treatments (Figure 1B). The Sr/Ca ratio at 32 °C had the highest fluctuation in values compared to 27 °C, where Sr/Ca ratios at 27 °C treatments (2.63 ± 0.01 mmol/mol, mean ± SE) were slightly higher than for the 32 °C treatments (2.62 ± 0.01 mmol/mol, mean ± SE) (Figure 1B). Inter-individual variability of Sr/Ca ratios were substantially higher for medium and high pCO_2 treatments (1052 µatm, 2066 µatm) compared to low pCO_2 (455 µatm) treatments; this was the case at both temperature levels (Figure 1B). No significant response of Sr/Ca ratio to differences in the pCO_2 and temperature as combined or as sole stressors (Table 2). However, skeletal Sr/Ca ratios were significantly altered over incubation time (p = 0.006, Table 2), with increasing values from samples taken after 45 days compared to those collected after 90 days.

Ca_{norm} ratios showed relatively variable values, which ranged between 647.74 mg/g and 755.30 mg/g across all treatments (Figure 2A). Ca_{norm} ratios were changed over the incubation time (p = 0.036, Table 2). The Ca_{norm} ratios at 27 °C rose from 699.73 ± 5.41 mg/g (mean ± SE) at 45 days to 709.02 ± 4.33 mg/g (mean ± SE) at 90 days incubation time (enhanced 1.33%), whereas the Ca_{norm} ratios at 32 °C rose from 693.51 ± 8.93 mg/g (mean ± SE) at 45 days to 712.60 ± 7.48 mg/g (mean ± SE) at 90 days incubation time (enhanced 2.74%). Ca_{norm} ratios were not significantly affected by temperature (p = 0.838, Table 2) or pCO_2 (p = 0.307, Table 2) as a single factor, nor as a combined factor (p = 0.250, Table 2).

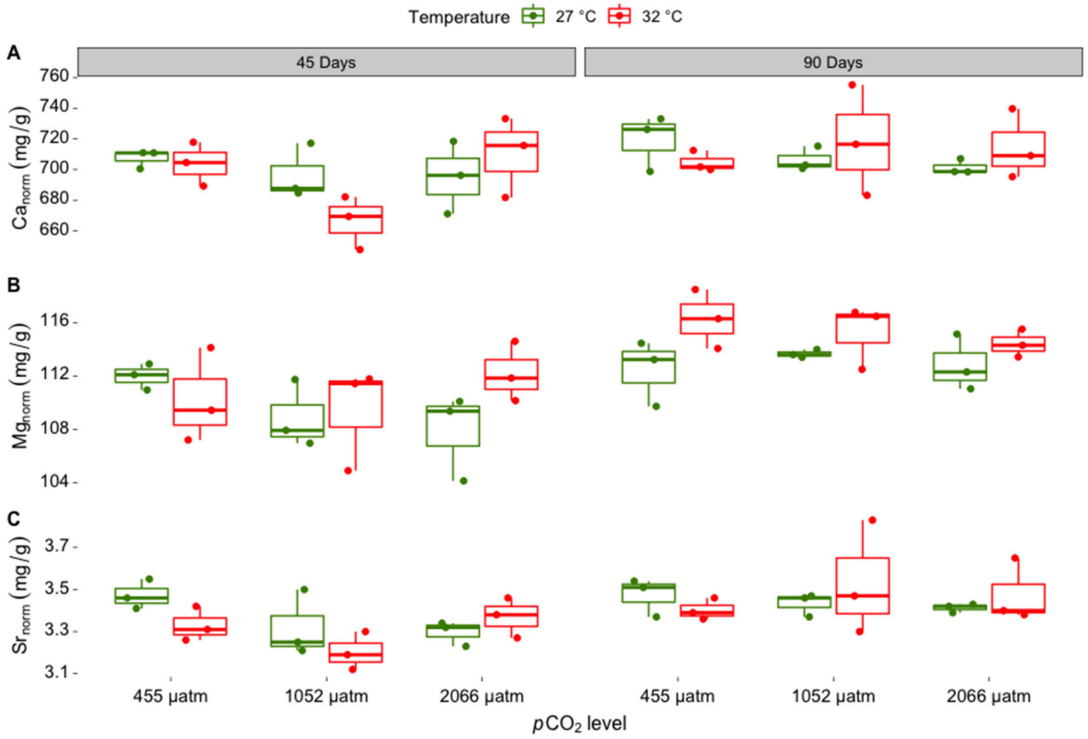

Figure 2. Ratios between skeletal mineral element to total skeletal material (**A**) Ca_{norm} ratios (mg/g), (**B**) Mg_{norm} ratios (mg/g), and (**C**) Sr_{norm} ratios (mg/g) in *A. yairi* exposed to elevated temperatures levels (27 °C and 32 °C) crossed with increased pCO_2 concentrations (455 µatm, 1052 µatm and 2066 µatm) measured after 45 and 90 days of incubation (n = 36). Dots represent individual skeletal mineral values, displayed with jitter to avoid overlap.

Mg_{norm} ratios from the skeleton of *A. yairi* were significantly altered by incubation time (p = 0.001, Table 2). Mg_{norm} ratios increased from 45 days to 90 days in both temperature treatment conditions (Figure 2B). At 27 °C, the Mg_{norm} ratios increased from 109.57 ± 0.94 mg/g (mean ± SE) at 45 days to 112.98 ± 0.57 mg/g (mean ± SE) at 90 days incubation time (i.e., 3.11% increase), while at 32 °C, the Mg_{norm} ratios increased from 110.61 ± 1.04 mg/g (mean ± SE) at 45 days to 115.31 ± 0.63 mg/g (mean ± SE) at 90 days incubation time (4.25% increase). There was no significant effect of pCO_2 nor any combined effect of the factors (Table 2). However, temperature led to a marginal increase in the Mg_{norm} ratios (p = 0.051, Table 2).

Sr_{norm} ratios were altered over incubation time (p = 0.005, Table 2) at both temperature treatments (Figure 2B). The mean value of the Sr_{norm} ratio at 27 °C increased by 2.38% from day 45 (3.36 ± 0.04 mg/g, mean ± SE) to day 90 (3.44 ± 0.02 mg/g, mean ± SD). Similarly, the mean value of Sr_{norm} ratio at 32 °C increased from 45 days (mean ± SD, 3.30 ± 0.04 mg/g) to 90 days (3.47 ± 0.06 mg/g, mean ± SD) incubation time (5.15% increase). However, there was no significant effect of combined stressor factors nor solely stressor factors on Sr_{norm} ratios (Table 2).

3.2. Skeletal Microstructure

High magnification SEM micrographs showed marked differences in skeletal structure between low pCO_2 (455 µatm) compared to medium and high pCO_2 treatments (1052 µatm, 2066 µatm, respectively) at both ambient and high temperatures (27 °C, 32 °C, respectively). The skeletal structure in low pCO_2 crossed with ambient (27 °C: 455 µatm) and high temperatures (32 °C: 455 µatm) revealed no remarkable differences between 45-day and 90-day incubation time. The stereom pores were arranged equally in shape and the aperture pores of the inner matrix were relatively equal in shape, while the trabecular surface was smooth (Figure 2A,B,G,H and Table 3).

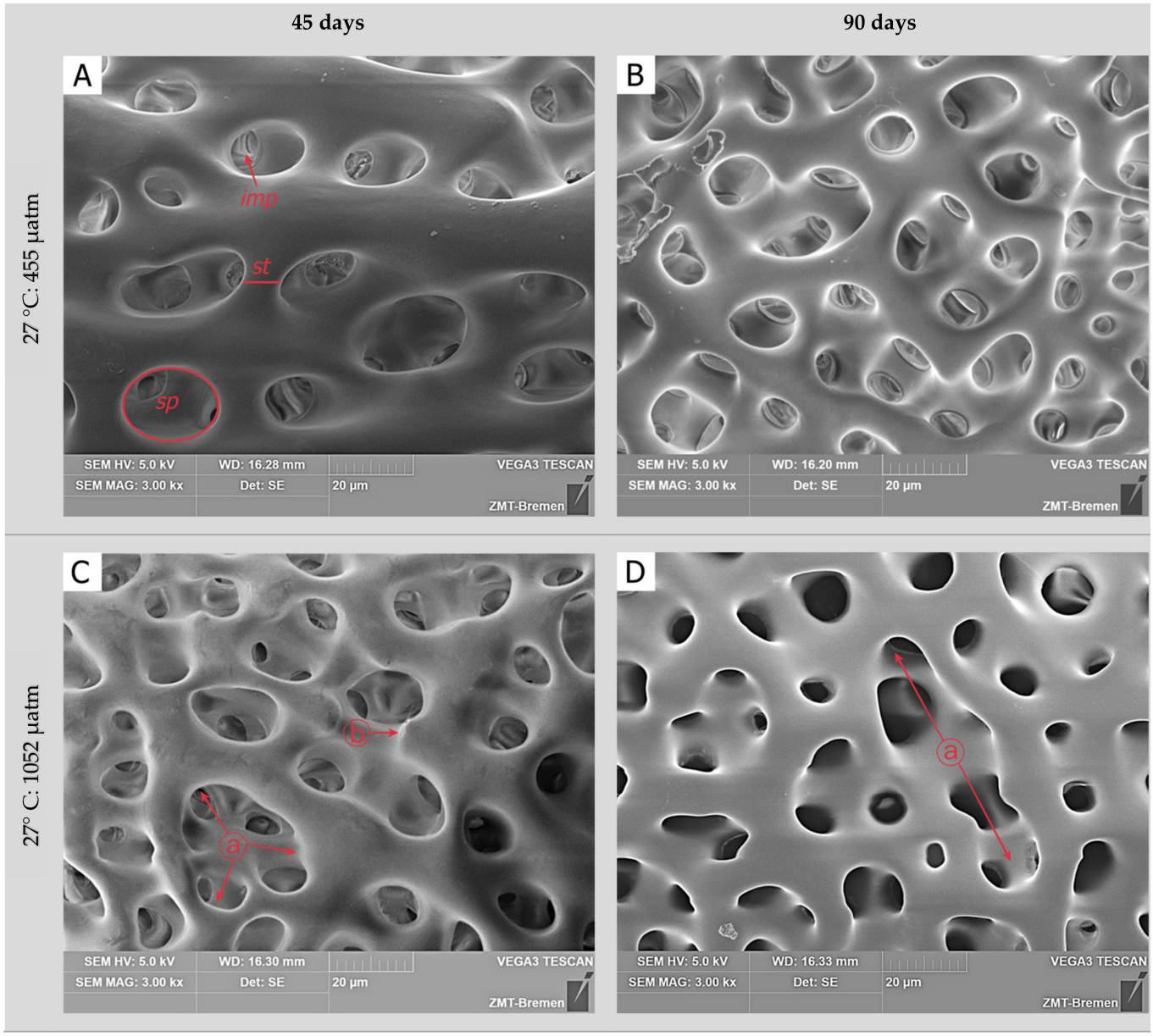

Figure 2. *Cont.*

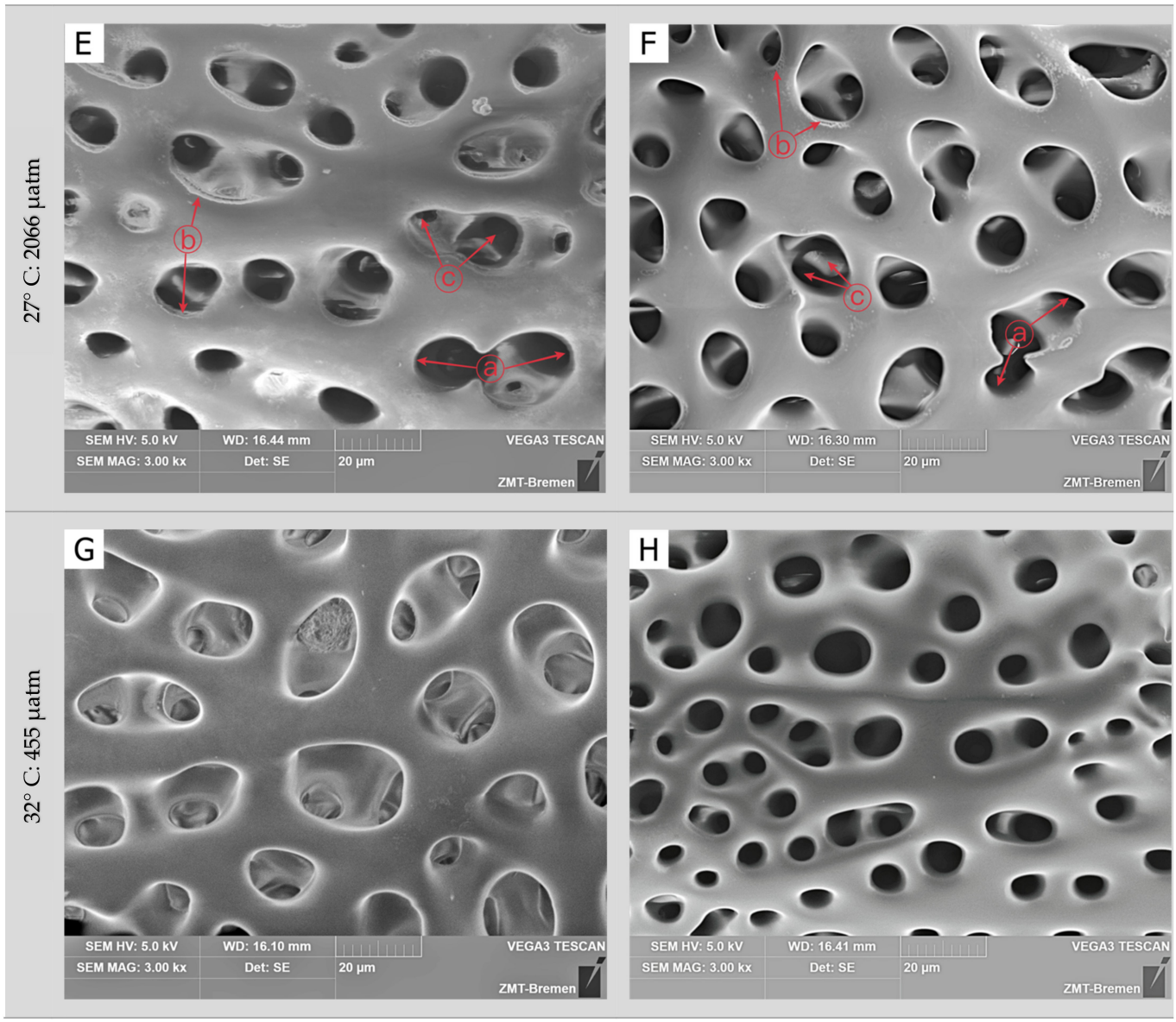

Figure 2. *Cont.*

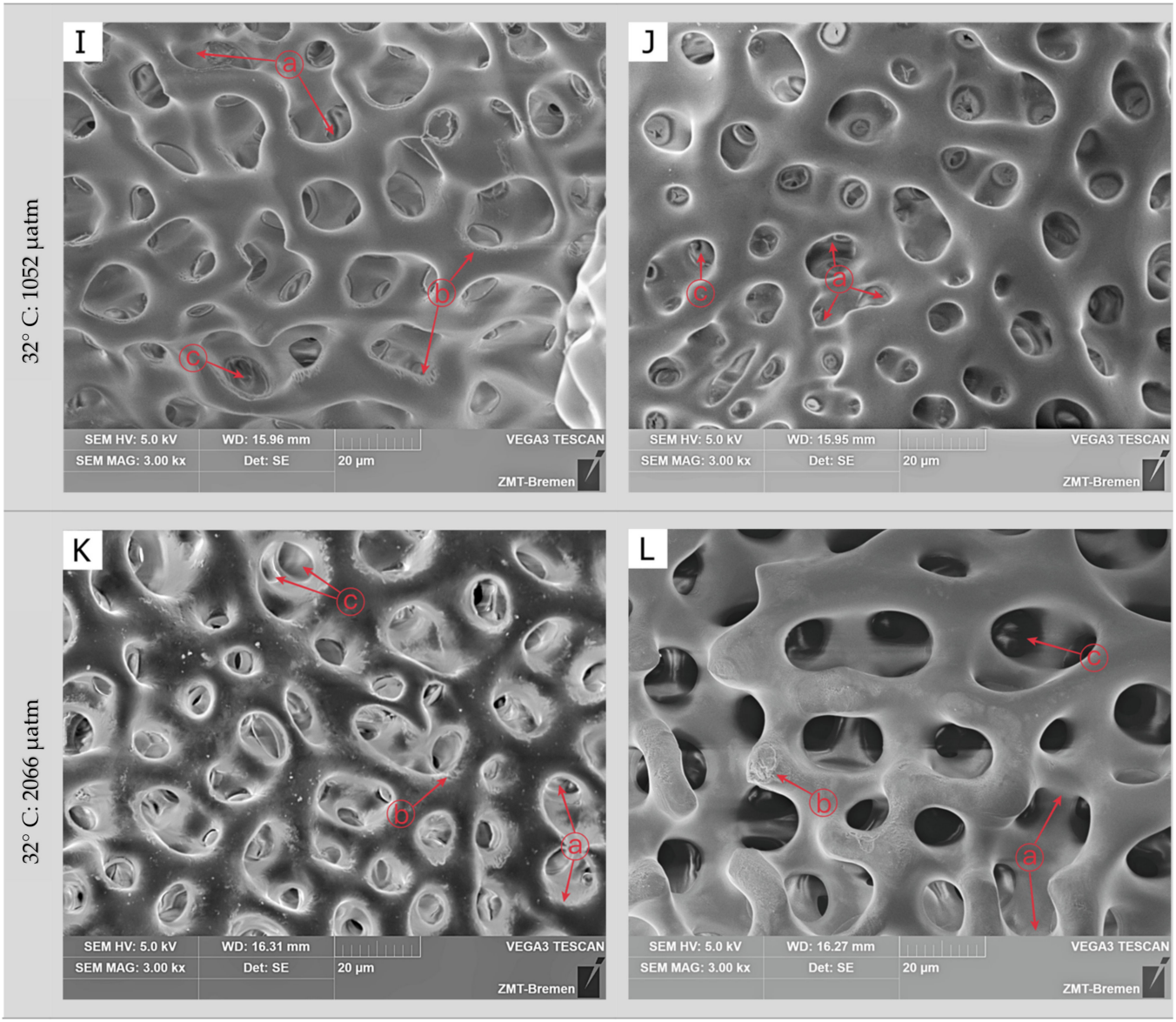

Figure 2. SEM micrographs of the skeletal microstructure of *A. yairi* cultured under two temperature levels (27 °C and 32 °C) crossed with three pCO_2 concentrations (455 µatm, 1052 µatm and 2066 µatm). Stereom microstructure after 45 (**A**,**C**,**E**,**G**,**I**,**K**) and 90 days (**B**,**D**,**F**,**H**,**J**,**L**) of incubation time. *sp*: stereom pore; *st*: skeleton trabeculae; *imp*: stereom inner matrix pore; (a) the galleries stereom pores are less-equal in shape; (b) dissolution in calcium carbonate skeleton; (c) increased size of inner matrix aperture pores. Technical image acquisition, SEM mode: SE, SEM HV: 5.0 kV, SEM magnification: 3000×.

In contrast, after 45-day and 90-day incubation times, the skeleton from medium and high pCO_2 treatments at ambient temperatures showed stereom structures that were more variable in shape compared to the control treatment, and signs of degradation, i.e., dissolution, were observed on the surface of the trabeculae (Figure 2C–F and Table 3). Furthermore, under high temperatures, these medium and high pCO_2 treatments in addition result in signs of skeletal degradation observed at the trabeculae surface, while the apertures of the inner matrix pores were wider (i.e., un-equal in shape) compared to the control treatment and the ambient temperature crossed with medium and high pCO_2 treatments (Figure 2I–L and Table 3).

Table 3. Skeletal microstructure characteristics of *A. yairi* under crossed temperatures and pCO_2 conditions at different incubation times as observed with scanning electron microscopy (SEM). ND: the skeleton surface is smooth and has no signs of degradation; DS: the skeleton surface had degradation signs; HD: the skeleton surface had high degradation signs; ES: the stereom pores were equal in shape; US: the stereom pores were un-equal in shape; HU: the stereom pores were highly un-equal in shape; EP: the inner matrix aperture pores were relatively equal in shape; UP: the inner matrix aperture pores were relatively un-equal in shape (wider). (n = 12).

Incubation Time	Temperature	pCO_2	Skeletal Surface	Stereom Pores	Inner Matrix Pores
45 days	27 °C	455 µatm	ND	ES	EP
		1052 µatm	DS	US	EP
		2066 µatm	DS	US	UP
	32 °C	455 µatm	ND	ES	EP
		1052 µatm	DS	US	UP
		2066 µatm	HD	HU	UP
90 days	27 °C	455 µatm	ND	ES	EP
		1052 µatm	DS	US	EP
		2066 µatm	DS	US	UP
	32 °C	455 µatm	ND	ES	EP
		1052 µatm	DS	US	UP
		2066 µatm	HD	HU	UP

4. Discussion

Our results imply that temperature plays a primary regulatory role in Mg concentration in the skeletal carbonate of *A. yairi*, where the Mg/Ca ratios increase under high-temperatures. This corroborates results from previous studies that found higher Mg concentrations associated with higher temperatures in echinoid and asteroid species [23,24,74]. This temperature association was previously attributed to kinetic factors affecting ion discrimination [23] and also to the physiological mechanisms that control Mg absorption in cells [75] during the biomineralization process. The increased Mg content of HMC was connected to an amorphous calcium magnesium carbonate (ACMC) precursor [76,77]. At high temperatures, the aqueous Mg^{2+} solvation energy barrier becomes lower [78]; hence this condition might favor more Mg^{2+} to be incorporated into the calcite lattice, encouraging the formation of ACMC, which later transforms into HMC.

Echinoderms are generally considered relatively poor regulators of internal acid–base balance, where the range of regulatory capacities is species-specific [79]. In hypercapnic conditions (high pCO_2, low pH), echinoderms increase the bicarbonate concentration in their coelomic fluid and practice passive skeletal dissolution to support internal acid–base regulatory functions due to acidosis [80]. Higher Mg concentrations in the skeleton in conjunction with a degradation in the inner skeleton (see Section 3.2) due to skeletal dissolution, as documented in the current studies, support the assumption of a trade-off mechanism [65,81]. The released HMC mineral is then used as an active buffering mechanism to compensate for changes in internal pH that may help to avoid or reduce physiological impacts.

We noticed that no single (temperature or pCO_2) nor combined stressor treatment affected skeletal Sr (Sr/Ca and Sr_{norm}) in *A. yairi.* This contrasts with previous studies on the starfish *Asterias rubens* [49] and the sea urchin *Paracentrotus lividus* [25], which reported that the Sr/Ca ratio depended on temperature. These contrasting results indicate a species-specific skeletal Sr control mechanism in the echinoderm group that may respond to the stressors. The calcification rates might play an important role in skeletal Sr precipitation rather than direct dependence on temperature. It is difficult to discriminate the effects of temperature and pCO_2 on skeletal Sr. Our data indicated that the skeletal Sr was increased over incubation time in all treatment combinations (electronic Supplementary Materials Figure S2) except the 27 °C: 455 µatm treatment, assuming that temperature and pCO_2 might have an indirect effect on skeletal Sr through their control over the

calcification process [23,34,69,82], which are common in biogenic calcites [83,84]. However, the incorporation pathways of Sr into the echinoderm ACC are still poorly understood, so further studies are needed.

We found a strong correlation between skeletal Sr and skeletal Mg ($R^2 = 0.04$, $p < 0.001$, electronic Supplementary Materials Figure S3), as Sr_{norm} increases with increasing Mg_{norm} ratio. Hence, Mg might play a role in affecting the Sr precipitation. Sr ions cannot easily substitute for Ca ions due to differences in cations ions size and weight (Sr^{2+} ionic radius of 1.18 Å: Ca^{2+} ionic radius of 1.00 Å [85]), which makes them incompatible in calcite [86]. High concentrations of Mg^{2+} (ionic radius of 0.72 Å [85]) that are incorporated in inorganic calcite can distort the crystal lattice (i.e., lattice deformation), which increases the size of calcium lattice positions and thus allows for increased incorporation of Sr^{2+} [87].

Similar to skeletal Sr, we found no direct influence of temperature or pCO_2 on the Ca_{norm} ratio (Table 2). However, the highest inter-individual variability of Ca_{norm} indicates that temperature and/or pCO_2 considerably alter the production of skeletal Ca in *A. yairi*, where Ca_{norm} ratios exhibited an increase with incubation time, except for the treatment of 27 °C: 455 µatm (~703 mg/g) where the ratio was relatively unchanged (electronic Supplementary Materials Figure S4). $CaCO_3$ is more soluble at lower temperatures [88] and high pCO_2 [20]. Under OW conditions, starfish seem to be able to boost their capacity to control calcification through the modulation of the intracellular calcifying fluids pH to produce $CaCO_3$. This might provide them with higher resistance and resilience towards the effects of OA. The increased energetic costs of this physiological response are indicated by elevated respiration rates [65]. Hence, in the long term, this phenotypic plasticity and biocalcification control mechanism might have further physiological implications for the starfish.

The hypercapnic conditions of the high pCO_2 treatment in our experiment have resulted in visible adverse effects on the skeletal structures in both ambient as well as elevated temperatures (Figure 2, Table 3). We detected changes in the stereom pores, the inner matrix pores and degradation of the skeleton surface through reduced deposition or dissolution, which increased over incubation time in the starfish that were exposed to medium and high pCO_2. These skeletal alterations might be due to the thin layer of epithelial tissue covering the starfish body wall [89], which acts as a protective membrane between the skeleton and the seawater [90]. Furthermore, the degradation of the epithelial tissue could also explain why the combination of OW with OA enhances the degradation of the skeletal structure that was observed in the high pCO_2 treatment (32 °C: 2066 µatm). We hypothesize that the epithelial tissue might become weaker in its function due to degradation of the epithelium cells during long-term experiments. Epithelial tightness is controlled by a protein series that molds a seal among epithelial cells [90], which are sensitive to elevated temperature.

The seawater chemistry factor, which was underlying the altered skeletal structure in *A. yairi* might involve calcium carbonate saturation state (Ω). Skeletal degradation provides evidence that the skeleton of *A. yairi* was negatively affected by lowered calcite saturation state (Ω_{ca}) as a function of increasing pCO_2 (Table 1), which directly affects the biomineralization and dissolution of the $CaCO_3$ in skeletal structures [17,91]. Near Ω_{ca} ~3, we found stereom alteration and degradation signs in trabeculae, which indicates that *A. yairi* was facing difficulty in producing and maintaining their skeleton compared to low pCO_2 treatments ($\Omega_{ca} > 5$). Previous studies found that the skeletal morphometric development of echinoid (e.g., sea urchin *Lytechinus variegatus*) was significantly affected by Ω_{ca} 2.53 [92]. Furthermore, increased susceptibility of the skeleton to dissolution through OA was suggested to be due to the skeleton composed of HMC, which is 30 times more soluble than pure calcite [47,93]. When the qualitative approach depicts changes in the skeleton micro-morphology because of exposure to elevated pCO_2 and temperature (Table 3, Figure 2), further investigation using quantitative analysis (e.g., stereom and inner matrix pore size) is required to quantify the alteration magnitude in skeleton microstructure as the deleterious impact of OA and OW [94,95].

Under OW and OA scenarios, calcifying marine organisms are expected to face unfavorable conditions to produce and maintain their skeletal HMC in order to sustain their biomechanical functions. Phenotypic plasticity requires re-allocation of energy as a trade-off and may represent a potential key mechanism for species viability [96]. For *A. yairi*, this mechanism might reflect strategies to maintain their skeletal HMC in a low pH environment by modulating their cellular chemistry to create isolated microenvironments of deposition, producing the specific mineral they necessitate, which involves significant energy re-allocation [97]. Since the asterinid starfish produces HMC, which is more soluble than calcite and aragonite, it signifies that more energy will be required to preserve the calcification process as the mechanism in both constructing and maintaining their skeletal components, leading to energy trade-offs against other physiological processes [65,98].

Changes in the shape of the stereom pores and degradation of the starfish skeleton potentially have implications for skeletal strength, stiffness, and function. Weakening of the structure possibly will reduce locomotion performance and result in a lower ability to resist predators and to face ocean currents, which then conveys consequences to the benthic community structure.

Supplementary Materials: The following supporting information can be downloaded at: https://www.mdpi.com/article/10.3390/jmse10081065/s1; Table S1: Tukey HSD post hoc test for the interactive effects of incubation time (45 and 90 days), pCO_2 (455 µatm, 1052 µatm, 2066 µatm) and temperature (27 °C, 32 °C) on skeletal Mg/Ca ratio of *A. yairi* using the 'agricolae R-package' for multiple comparisons to interrogate the main effects of incubation time, temperature and pCO_2 (incubation time: pCO_2: temperature = 0.014, Table 2); Figure S1: Schematic of ocean acidification and ocean warming experimental design with a fully factorial combination of low pCO_2 (455 µatm), moderate pCO_2 (1052 µatm), and high pCO_2 (2066 µatm) treatments with ambient temperature (27 °C) and high temperature (32 °C) treatments; Figure S2: Skeletal Sr values over incubation time in *A. yairi* exposed to elevated temperatures levels (27 °C and 32 °C) crossed with increased pCO_2 concentrations (455 µatm, 1052 µatm, and 2066 µatm). (**A**) Sr/Ca ratio (mmol/mol), (**B**) Sr_{norm} ratio (mg/g). Data were presented as mean (n = 36); Figure S3: Correlation of Sr_{norm} ratios (mg/g) against Mg_{norm} ratios (mg/g) (R^2 = 0.44, $F_{1, 34}$ = 26.78, $p = 1.019 \times 10^{-5}$) in *A. yairi* exposed to elevated temperatures levels (27 °C and 32 °C) crossed with increased pCO_2 concentrations (455 µatm, 1052 µatm, and 2066 µatm). (n = 36); Figure S4: Skeletal Ca_{norm} (mg/g) ratio over incubation time in *A. yairi* exposed to elevated temperatures levels (27 °C and 32 °C) crossed with increased pCO_2 concentrations (455 µatm, 1052 µatm, and 2066 µatm). Data were presented as mean (n = 36). For more details, please see [66,99–106].

Author Contributions: Conceptualized and designed: M.K. and H.W.; methodology: M.K., S.S.D., M.S. and H.W.; investigation: M.K.; resources: M.K. and H.W.; sample processing and analysis: M.K.; data curation: M.K.; writing original draft preparation: M.K.; visualization: M.K.; writing-review and editing: M.K., S.S.D., M.S. and H.W.; supervision: H.W. All authors have read and agreed to the published version of the manuscript.

Funding: This research project was supported by the Academy Doctoral Research—Grant Leibniz Centre for Tropical Marine Research (ZMT), Germany and the Ministry of Education, Culture, Research, and Technology (MoECRT), Republic of Indonesia—Asian Development Bank (ADB) AKSI Project [grant number L3749-INO] to M.K.

Institutional Review Board Statement: Not applicable.

Informed Consent Statement: Not applicable.

Data Availability Statement: The datasets used and analyzed during the current study are present in the manuscript and/or supplementary materials. Data are available upon request from the corresponding author.

Acknowledgments: We would like to thank Andreas Kunzmann (ZMT, Bremen, Germany) for his advice on the starfish *A. yairi* as a model organism. Many thanks are due to the ZMT laboratory staff, namely Jule Mawick, Sebastian Flotow, Silvia Hardenberg, José Garcia, Nico Steinel, Matthias Birkicht and Fabian Hüge.

Conflicts of Interest: On behalf of all authors, the corresponding author states that there is no conflict of interest.

References

1. Watson, A.J.; Schuster, U.; Shutler, J.D.; Holding, T.; Ashton, I.G.C.; Landschutzer, P.; Woolf, D.K.; Goddijn-Murphy, L. Revised estimates of ocean-atmosphere CO_2 flux are consistent with ocean carbon inventory. *Nat. Commun.* **2020**, *11*, 4422. [CrossRef] [PubMed]
2. Feely, R.A.; Sabine, C.L.; Lee, K.; Berelson, W.; Kleypas, J.; Fabry, V.J.; Millero, F.J. Impact of anthropogenic CO_2 on the $CaCO_3$ system in the oceans. *Science* **2004**, *305*, 362–366. [CrossRef] [PubMed]
3. Sabine, C.L.; Feely, R.A.; Gruber, N.; Key, R.M.; Lee, K.; Bullister, J.L.; Wanninkhof, R.; Wong, C.S.; Wallace, D.W.; Tilbrook, B.; et al. The oceanic sink for anthropogenic CO_2. *Science* **2004**, *305*, 367–371. [CrossRef]
4. Orr, J.C.; Fabry, V.J.; Aumont, O.; Bopp, L.; Doney, S.C.; Feely, R.A.; Gnanadesikan, A.; Gruber, N.; Ishida, A.; Joos, F.; et al. Anthropogenic ocean acidification over the twenty-first century and its impact on calcifying organisms. *Nature* **2005**, *437*, 681–686. [CrossRef]
5. Hoegh-Guldberg, O.; Bruno, J.F. The impact of climate change on the world's marine ecosystems. *Science* **2010**, *328*, 1523–1528. [CrossRef] [PubMed]
6. Dupont, S.; Ortega-Martinez, O.; Thorndyke, M. Impact of near-future ocean acidification on echinoderms. *Ecotoxicology* **2010**, *19*, 449–462. [CrossRef] [PubMed]
7. Rodolfo-Metalpa, R.; Lombardi, C.; Cocito, S.; Hall-Spencer, J.M.; Gambi, M.C. Effects of ocean acidification and high temperatures on the bryozoan *Myriapora truncata* at natural CO_2 vents. *Mar. Ecol.* **2010**, *31*, 447–456. [CrossRef]
8. Matranga, V.; Bonaventura, R.; Costa, C.; Karakostis, K.; Pinsino, A.; Russo, R.; Zito, F. Echinoderms as Blueprints for Biocalcification: Regulation of Skeletogenic Genes and Matrices. In *Molecular Biomineralization: Aquatic Organisms Forming Extraordinary Materials*; Müller, W.E.G., Ed.; Springer: Berlin/Heidelberg, Germany, 2011; pp. 225–248.
9. Mann, S. *Mineralization in Biological Systems*; Springer: Berlin/Heidelberg, Germany, 1983; pp. 125–174.
10. Killian, C.E.; Wilt, F.H. Molecular aspects of biomineralization of the echinoderm endoskeleton. *Chem. Rev.* **2008**, *108*, 4463–4474. [CrossRef]
11. Gorzelak, P. *Functional Micromorphology of the Echinoderm Skeleton*; Cambridge University Press: Cambridge, UK, 2021; p. 44.
12. Feng, Q. Principles of Calcium-Based Biomineralization. In *Molecular Biomineralization: Aquatic Organisms Forming Extraordinary Materials*; Müller, W.E.G., Ed.; Springer: Berlin/Heidelberg, Germany, 2011; pp. 141–197.
13. Gilbert, P.U.P.A.; Wilt, F.H. Molecular Aspects of Biomineralization of the Echinoderm Endoskeleton. In *Molecular Biomineralization: Aquatic Organisms Forming Extraordinary Materials*; Müller, W.E.G., Ed.; Springer: Berlin/Heidelberg, Germany, 2011; pp. 199–223.
14. Ries, J.B.; Ghazaleh, M.N.; Connolly, B.; Westfield, I.; Castillo, K.D. Impacts of seawater saturation state (ΩA = 0.4–4.6) and temperature (10, 25 °C) on the dissolution kinetics of whole-shell biogenic carbonates. *Geochim. Cosmochim. Acta* **2016**, *192*, 318–337. [CrossRef]
15. Kawahata, H.; Fujita, K.; Iguchi, A.; Inoue, M.; Iwasaki, S.; Kuroyanagi, A.; Maeda, A.; Manaka, T.; Moriya, K.; Takagi, H.; et al. Perspective on the response of marine calcifiers to global warming and ocean acidification—Behavior of corals and foraminifera in a high CO_2 world "hot house". *Prog. Earth Planet Sci.* **2019**, *6*, 5. [CrossRef]
16. Morse, J.W.; Andersson, A.J.; Mackenzie, F.T. Initial responses of carbonate-rich shelf sediments to rising atmospheric pCO_2 and "ocean acidification": Role of high Mg-calcites. *Geochim. Cosmochim. Acta* **2006**, *70*, 5814–5830. [CrossRef]
17. Watson, S.A.; Peck, L.S.; Tyler, P.A.; Southgate, P.C.; Tan, K.S.; Day, R.W.; Morley, S.A. Marine invertebrate skeleton size varies with latitude, temperature and carbonate saturation: Implications for global change and ocean acidification. *Glob. Chang. Biol.* **2012**, *18*, 3026–3038. [CrossRef] [PubMed]
18. Anand, M.; Rangesh, K.; Maruthupandy, M.; Jayanthi, G.; Rajeswari, B.; Priya, R.J. Effect of CO_2 driven ocean acidification on calcification, physiology and ovarian cells of tropical sea urchin *Salmacis virgulata*—A microcosm approach. *Heliyon* **2021**, *7*, e05970. [CrossRef] [PubMed]
19. Duquette, A.; McClintock, J.B.; Amsler, C.D.; Perez-Huerta, A.; Milazzo, M.; Hall-Spencer, J.M. Effects of ocean acidification on the shells of four Mediterranean gastropod species near a CO_2 seep. *Mar. Pollut. Bull.* **2017**, *124*, 917–928. [CrossRef]
20. Ries, J.B.; Cohen, A.L.; McCorkle, D.C. Marine calcifiers exhibit mixed responses to CO_2-induced ocean acidification. *Geology* **2009**, *37*, 1131–1134. [CrossRef]
21. Pörtner, H. Ecosystem effects of ocean acidification in times of ocean warming: A physiologist's view. *Mar. Ecol. Prog. Ser.* **2008**, *373*, 203–217. [CrossRef]
22. Weiner, S.; Dove, P.M. An overview of biomineralization processes and the problem of the vital effect. *Rev. Mineral. Geochem.* **2003**, *54*, 1–29. [CrossRef]
23. Weber, J.N. Temperature dependence of magnesium in echinoid and asteroid skeletal calcite: A reinterpretation of its significance. *J. Geol.* **1973**, *81*, 543–556. [CrossRef]
24. Chave, K.E. Aspects of the biogeochemistry of magnesium 1. Calcareous marine organisms. *J. Geol.* **1954**, *62*, 266–283. [CrossRef]
25. Hermans, J.; Borremans, C.; Willenz, P.; André, L.; Dubois, P. Temperature, salinity and growth rate dependences of Mg/Ca and Sr/Ca ratios of the skeleton of the sea urchin *Paracentrotus lividus* (Lamarck): An experimental approach. *Mar. Biol.* **2010**, *157*, 1293–1300. [CrossRef]

26. Duquette, A.; Vohra, Y.K.; McClintock, J.B.; Angus, R.A. Near-future temperature reduces Mg/Ca ratios in the major skeletal components of the common subtropical sea urchin *Lytechinus variegatus*. *J. Exp. Mar. Biol. Ecol.* **2018**, *509*, 1–7. [CrossRef]
27. Lowenstam, H.A.; Weiner, S. *On Biomineralization*; Oxford University Press: New York, NY, USA, 1989.
28. Gazeau, F.; Parker, L.M.; Comeau, S.; Gattuso, J.-P.; O'Connor, W.A.; Martin, S.; Pörtner, H.-O.; Ross, P.M. Impacts of ocean acidification on marine shelled molluscs. *Mar. Biol.* **2013**, *160*, 2207–2245. [CrossRef]
29. Olson, I.C.; Kozdon, R.; Valley, J.W.; Gilbert, P.U. Mollusk shell nacre ultrastructure correlates with environmental temperature and pressure. *J. Am. Chem. Soc.* **2012**, *134*, 7351–7358. [CrossRef] [PubMed]
30. Reynaud, S.; Ferrier-Pagès, C.; Meibom, A.; Mostefaoui, S.; Mortlock, R.; Fairbanks, R.; Allemand, D. Light and temperature effects on Sr/Ca and Mg/Ca ratios in the scleractinian coral *Acropora* sp. *Geochim. Cosmochim. Acta* **2007**, *71*, 354–362. [CrossRef]
31. Toyofuku, T.; Kitazato, H.; Kawahata, H.; Tsuchiya, M.; Nohara, M. Evaluation of Mg/Ca thermometry in foraminifera: Comparison of experimental results and measurements in nature. *Paleoceanography* **2000**, *15*, 456–464. [CrossRef]
32. Dissard, D.; Nehrke, G.; Reichart, G.J.; Bijma, J. The impact of salinity on the Mg/Ca and Sr/Ca ratio in the benthic foraminifera *Ammonia tepida*: Results from culture experiments. *Geochim. Cosmochim. Acta* **2010**, *74*, 928–940. [CrossRef]
33. Bell, T.; Nishida, K.; Ishikawa, K.; Suzuki, A.; Nakamura, T.; Sakai, K.; Ohno, Y.; Iguchi, A.; Yokoyama, Y. Temperature-controlled culture experiments with primary polyps of coral *Acropora digitifera*: Calcification rate variations and skeletal Sr/Ca, Mg/Ca, and Na/Ca ratios. *Palaeogeogr. Palaeoclimatol. Palaeoecol.* **2017**, *484*, 129–135. [CrossRef]
34. Kısakürek, B.; Eisenhauer, A.; Böhm, F.; Garbe-Schönberg, D.; Erez, J. Controls on shell Mg/Ca and Sr/Ca in cultured planktonic foraminiferan, *Globigerinoides ruber* (white). *Earth Planet Sci. Lett.* **2008**, *273*, 260–269. [CrossRef]
35. Rathburn, A.E.; De Deckker, P. Magnesium and strontium compositions of recent benthic foraminifera from the Coral Sea, Australia and Prydz Bay, Antarctica. *Mar. Micropaleontol.* **1997**, *32*, 231–248. [CrossRef]
36. Dodd, J.R. Magnesium and strontium in calcareous skeletons: A review. *J. Paleontol.* **1967**, *41*, 1313–1329.
37. Kolbuk, D.; Di Giglio, S.; M'Zoudi, S.; Dubois, P.; Stolarski, J.; Gorzelak, P. Effects of seawater Mg^{2+}/Ca^{2+} ratio and diet on the biomineralization and growth of sea urchins and the relevance of fossil echinoderms to paleoenvironmental reconstructions. *Geobiology* **2020**, *18*, 710–724. [CrossRef] [PubMed]
38. LaVigne, M.; Hill, T.M.; Sanford, E.; Gaylord, B.; Russell, A.D.; Lenz, E.A.; Hosfelt, J.D.; Young, M.K. The elemental composition of purple sea urchin (*Strongylocentrotus purpuratus*) calcite and potential effects of pCO_2 during early life stages. *Biogeosciences* **2013**, *10*, 3465–3477. [CrossRef]
39. Todgham, A.E.; Stillman, J.H. Physiological responses to shifts in multiple environmental stressors: Relevance in a changing world. *Integr. Comp. Biol.* **2013**, *53*, 539–544. [CrossRef] [PubMed]
40. Harvey, B.P.; Gwynn-Jones, D.; Moore, P.J. Meta-analysis reveals complex marine biological responses to the interactive effects of ocean acidification and warming. *Ecol. Evol.* **2013**, *3*, 1016–1030. [CrossRef] [PubMed]
41. Kroeker, K.J.; Kordas, R.L.; Crim, R.; Hendriks, I.E.; Ramajo, L.; Singh, G.S.; Duarte, C.M.; Gattuso, J.-P. Impacts of ocean acidification on marine organisms: Quantifying sensitivities and interaction with warming. *Glob. Chang. Biol.* **2013**, *19*, 1884–1896. [CrossRef] [PubMed]
42. Brahmi, C.; Chapron, L.; Le Moullac, G.; Soyez, C.; Beliaeff, B.; Lazareth, C.E.; Gaertner-Mazouni, N.; Vidal-Dupiol, J. Effects of elevated temperature and pCO_2 on the respiration, biomineralization and photophysiology of the giant clam *Tridacna maxima*. *Conserv. Physiol.* **2021**, *9*, coab041. [CrossRef]
43. Knights, A.M.; Norton, M.J.; Lemasson, A.J.; Stephen, N. Ocean acidification mitigates the negative effects of increased sea temperatures on the biomineralization and crystalline ultrastructure of *Mytilus*. *Front. Mar. Sci.* **2020**, *7*. [CrossRef]
44. Li, S.; Liu, C.; Huang, J.; Liu, Y.; Zheng, G.; Xie, L.; Zhang, R. Interactive effects of seawater acidification and elevated temperature on biomineralization and amino acid metabolism in the mussel *Mytilus edulis*. *J. Exp. Biol.* **2015**, *218*, 3623–3631. [CrossRef]
45. Byrne, M.; Smith, A.M.; West, S.; Collard, M.; Dubois, P.; Graba-landry, A.; Dworjanyn, S.A. Warming influences Mg^{2+} content, while warming and acidification influence calcification and test strength of a sea urchin. *Environ. Sci. Technol.* **2014**, *48*, 12620–12627. [CrossRef]
46. Byrne, M. Impact of ocean warming and ocean acidification on marine invertebrate life history stages: Vulnerabilities and potential for persistence in a changing ocean. In *Oceanography and Marine Biology: An Annual Review*; Gibson, R.N., Atkinson, R.J.A., Gordon, J.D.M., Smith, I.P., Hughes, D.J., Eds.; Taylor & Francis: Boca Raton, FL, USA, 2011; pp. 1–42.
47. Politi, Y.; Arad, T.; Klein, E.; Weiner, S.; Addadi, L. Sea urchin spine calcite forms via a transient amorphous calcium carbonate phase. *Science* **2004**, *306*, 1161–1164. [CrossRef]
48. Kokorin, A.I.; Mirantsev, G.V.; Rozhnov, S.V. General features of echinoderm skeleton formation. *Paleontol. J.* **2015**, *48*, 1532–1539. [CrossRef]
49. Borremans, C.; Hermans, J.; Baillon, S.; André, L.; Dubois, P. Salinity effects on the Mg/Ca and Sr/Ca in starfish skeletons and the echinoderm relevance for paleoenvironmental reconstructions. *Geology* **2009**, *37*, 351–354. [CrossRef]
50. Dubois, P. The skeleton of postmetamorphic echinoderms in a changing world. *Biol. Bull.* **2014**, *226*, 223–236. [CrossRef] [PubMed]
51. Weiner, S. Organic matrixlike macromolecules associated with the mineral phase of sea urchin skeletal plates and teeth. *J. Exp. Zool.* **1985**, *234*, 7–15. [CrossRef] [PubMed]
52. Killian, C.E.; Wilt, F.H. Characterization of the proteins comprising the integral matrix of *Strongylocentrotus purpuratus* embryonic spicules. *J. Biol. Chem.* **1996**, *271*, 9150–9159. [CrossRef]

53. Addadi, L.; Weiner, S. Control and design principles in biological mineralization. *Angew. Chem. Int. Ed.* **1992**, *31*, 153–169. [CrossRef]
54. Hermans, J.; Andre, L.; Navez, J.; Pernet, P.; Dubois, P. Relative influences of solution composition and presence of intracrystalline proteins on magnesium incorporation in calcium carbonate minerals: Insight into vital effects. *J. Geophys. Res.* **2011**, *116*, G01001. [CrossRef]
55. Ries, J.B. A physicochemical framework for interpreting the biological calcification response to CO_2-induced ocean acidification. *Geochim. Cosmochim. Acta* **2011**, *75*, 4053–4064. [CrossRef]
56. Mackenzie, F.T.; Bischoff, W.D.; Bishop, F.C.; Loijens, M.; Schoonmaker, J.; Wollast, R. Magnesian Calcites: Low Temperature Occurrence, Solubility and Solid Solution Behavior. In *Carbonates: Mineralogy and Chemistry, Reviews in Mineralogy*; Richard, J.R., Ed.; Mineralogical Society of America: Stony Brook, NY, USA, 1983; Volume 11, pp. 97–144.
57. Knoll, A.H. Biomineralization and evolutionary history. *Rev. Mineral. Geochem.* **2003**, *54*, 329–356. [CrossRef]
58. Byrne, M.; Fitzer, S. The impact of environmental acidification on the microstructure and mechanical integrity of marine invertebrate skeletons. *Conserv. Physiol.* **2019**, *7*, coz062. [CrossRef]
59. Andersson, A.J.; Mackenzie, F.T.; Bates, N.R. Life on the margin: Implications of ocean acidification on Mg-calcite, high latitude and cold-water marine calcifiers. *Mar. Ecol. Prog. Ser.* **2008**, *373*, 265–273. [CrossRef]
60. O'Loughlin, P.M.; Rowe, F.W.E. A systematic revision of the asterinid genus *Aquilonastra* O'Loughlin, 2004 (Echinodermata: Asteroidea). *Mem. Mus. Vic.* **2006**, *63*, 257–287. [CrossRef]
61. Menge, B.A.; Sanford, E. Ecological role of sea stars from populations to meta ecosystems. In *Starfish: Biology and Ecology of the Asteroidea*; Lawrence, J.M., Ed.; The Johns Hopkins University Press: Baltimore, MD, USA, 2013; pp. 67–80.
62. Balogh, R.; Byrne, M. Developing in a warming intertidal, negative carry over effects of heatwave conditions in development to the pentameral starfish in *Parvulastra exigua*. *Mar. Environ. Res.* **2020**, *162*, 105083. [CrossRef] [PubMed]
63. Nguyen, H.D.; Byrne, M. Early benthic juvenile *Parvulastra exigua* (Asteroidea) are tolerant to extreme acidification and warming in its intertidal habitat. *J. Exp. Mar. Biol. Ecol.* **2014**, *453*, 36–42. [CrossRef]
64. McElroy, D.J.; Nguyen, H.D.; Byrne, M. Respiratory response of the intertidal seastar *Parvulastra exigua* to contemporary and near-future pulses of warming and hypercapnia. *J. Exp. Mar. Biol. Ecol.* **2012**, *416–417*, 1–7. [CrossRef]
65. Khalil, M.; Doo, S.S.; Stuhr, M.; Westphal, H. Leibniz Centre for Tropical Marine Research (ZMT), Bremen, Germany. 2022, Unpublished Work.
66. Dickson, A.G.; Sabine, C.L.; Christian, J.R. (Eds.) *Guide to Best Practices for Ocean CO_2 Measurements*; PICES Special Publication 3; North Pacific Marine Science Organization: British Columbia, Canada, 2007; Volume 3, p. 191.
67. Bray, L.; Pancucci-Papadopoulou, M.A.; Hall-Spencer, J.M. Sea urchin response to rising pCO_2 shows ocean acidification may fundamentally alter the chemistry of marine skeletons. *Mediterr. Mar. Sci.* **2014**, *15*, 510–519. [CrossRef]
68. Ehrlich, H.; Elkin, Y.N.; Artoukov, A.A.; Stonik, V.A.; Safronov, P.P.; Bazhenov, V.V.; Kurek, D.V.; Varlamov, V.P.; Born, R.; Meissner, H.; et al. Simple method for preparation of nanostructurally organized spines of sand dollar *Scaphechinus mirabilis* (Agassiz, 1863). *Mar. Biotechnol.* **2011**, *13*, 402–410. [CrossRef]
69. Russell, A.D.; Hönisch, B.; Spero, H.J.; Lea, D.W. Effects of seawater carbonate ion concentration and temperature on shell U, Mg, and Sr in cultured planktonic foraminifera. *Geochim. Cosmochim. Acta* **2004**, *68*, 4347–4361. [CrossRef]
70. R Core Team. *R: A Language and Environment for Statistical Computing*; R Foundation for Statistical Computing: Vienna, Austria, 2022.
71. Shapiro, S.S.; Wilk, M.B. An analysis of variance test for normality (complete samples). *Biometrika* **1965**, *52*, 591–611. [CrossRef]
72. Levene, H. Robust tests for equality of variances. In *Contributions to Probability and Statistics*; Olkin, I., Ed.; Stanford University Press: Palo Alto, CA, USA, 1960; pp. 278–292.
73. De Mendiburu, F. Agricolae: Statistical Procedures for Agricultural Research. R Package Version 1.3-5. 2021. Available online: https://CRAN.R-project.org/package=agricolae (accessed on 19 January 2022).
74. Weber, J.N. The incorporation of magnesium into the skeletal calcites of echinoderms. *Am. J. Sci.* **1969**, *267*, 537–566. [CrossRef]
75. Rosenthal, Y.; Boyle, E.A.; Slowey, N. Temperature control on the incorporation of magnesium, strontium, fluorine, and cadmium into benthic foraminiferal shells from Little Bahama Bank: Prospects for thermocline paleoceanography. *Geochim. Cosmochim. Acta* **1997**, *61*, 3633–3643. [CrossRef]
76. Purgstaller, B.; Mavromatis, V.; Goetschl, K.E.; Steindl, F.R.; Dietzel, M. Effect of temperature on the transformation of amorphous calcium magnesium carbonate with near-dolomite stoichiometry into high Mg-calcite. *CrystEngComm* **2021**, *23*, 1969–1981. [CrossRef]
77. Radha, A.V.; Fernandez-Martinez, A.; Hu, Y.; Jun, Y.-S.; Waychunas, G.A.; Navrotsky, A. Energetic and structural studies of amorphous $Ca_{1-x}Mg_xCO_3{\cdot}nH_2O$ ($0 \leq x \leq 1$). *Geochim. Cosmochim. Acta* **2012**, *90*, 83–95. [CrossRef]
78. Di Lorenzo, F.; Rodríguez-Galán, R.M.; Prieto, M. Kinetics of the solvent-mediated transformation of hydromagnesite into magnesite at different temperatures. *Mineral. Mag.* **2018**, *78*, 1363–1372. [CrossRef]
79. Stumpp, M.; Hu, M.Y. pH Regulation and Excretion in Echinoderms. In *Acid-Base Balance and Nitrogen Excretion in Invertebrates*; Weihrauch, D., O'Donnell, M., Eds.; Springer: Berlin/Heidelberg, Germany, 2017; pp. 261–273.
80. Miles, H.; Widdicombe, S.; Spicer, J.I.; Hall-Spencer, J. Effects of anthropogenic seawater acidification on acid-base balance in the sea urchin *Psammechinus miliaris*. *Mar. Pollut. Bull.* **2007**, *54*, 89–96. [CrossRef] [PubMed]

81. Asnaghi, V.; Mangialajo, L.; Gattuso, J.-P.; Francour, P.; Privitera, D.; Chiantore, M. Effects of ocean acidification and diet on thickness and carbonate elemental composition of the test of juvenile sea urchins. *Mar. Environ. Res.* **2014**, *93*, 78–84. [CrossRef]
82. Lorens, R.B. Sr, Cd, Mn and Co distribution coefficients in calcite as a function of calcite precipitation rate. *Geochim. Cosmochim. Acta* **1981**, *45*, 553–561. [CrossRef]
83. Lea, D.W.; Mashiotta, T.A.; Spero, H.J. Controls on magnesium and strontium uptake in planktonic foraminifera determined by live culturing. *Geochim. Cosmochim. Acta* **1999**, *63*, 2369–2379. [CrossRef]
84. Stoll, H.M.; Rosenthal, Y.; Falkowski, P. Climate proxies from Sr/Ca of coccolith calcite: Calibrations from continuous culture of *Emiliania huxleyi*. *Geochim. Cosmochim. Acta* **2002**, *66*, 927–936. [CrossRef]
85. Shannon, R.D. Revised effective ionic radii and systematic studies of interatomic distances in halides and chalcogenides. *Acta Cryst.* **1976**, *32*, 751–767. [CrossRef]
86. Tesoriero, A.J.; Pankow, J.F. Solid solution partitioning of Sr^{2+}, Ba^{2+}, and Cd^{2+} to calcite. *Geochim. Cosmochim. Acta* **1996**, *60*, 1053–1063. [CrossRef]
87. Mucci, A.; Morse, J.W. The incorporation of Mg^{2+} and Sr^{2+} into calcite overgrowths: Influences of growth rate and solution composition. *Geochim. Cosmochim. Acta* **1983**, *47*, 217–233. [CrossRef]
88. Zeebe, R.E.; Wolf-Gladrow, D. *CO_2 in Seawater: Equilibrium, Kinetics, Isotopes*; Elsevier: Amsterdam, The Netherlands, 2001.
89. Dubois, P.; Chen, C.P. Calcification in echinoderms. In *Echinoderm Studies*; Jangoux, M., Lawrence, J.M., Eds.; AA Balkema: Rotterdam, The Netherlands, 1989; Volume 3, pp. 109–178.
90. Melzner, F.; Mark, F.C.; Seibel, B.A.; Tomanek, L. Ocean acidification and coastal marine invertebrates: Tracking CO_2 effects from seawater to the cell. *Ann. Rev. Mar. Sci.* **2020**, *12*, 499–523. [CrossRef] [PubMed]
91. Feely, R.; Doney, S.; Cooley, S. Ocean acidification: Present conditions and future changes in a high-CO_2 world. *Oceanography* **2009**, *22*, 36–47. [CrossRef]
92. Challener, R.C.; McClintock, J.B.; Makowsky, R. Effects of reduced carbonate saturation state on early development in the common edible sea urchin *Lytechinus variegatus*: Implications for land-based aquaculture. *J. Appl. Aquac.* **2013**, *25*, 154–175. [CrossRef]
93. McClintock, J.B.; Amsler, M.O.; Angus, R.A.; Challener, R.C.; Schram, J.B.; Amsler, C.D.; Mah, C.L.; Cuce, J.; Baker, B.J. The Mg-Calcite composition of antarctic echinoderms: Important implications for predicting the impacts of ocean acidification. *J. Geol.* **2011**, *119*, 457–466. [CrossRef]
94. Johnson, R.; Harianto, J.; Thomson, M.; Byrne, M. The effects of long-term exposure to low pH on the skeletal microstructure of the sea urchin *Heliocidaris erythrogramma*. *J. Exp. Mar. Biol. Ecol.* **2020**, *523*, 151250. [CrossRef]
95. Hazan, Y.; Wangensteen, O.S.; Fine, M. Tough as a rock-boring urchin: Adult *Echinometra* sp. EE from the Red Sea show high resistance to ocean acidification over long-term exposures. *Mar. Biol.* **2014**, *161*, 2531–2545. [CrossRef]
96. Gibbin, E.M.; Massamba N'Siala, G.; Chakravarti, L.J.; Jarrold, M.D.; Calosi, P. The evolution of phenotypic plasticity under global change. *Sci. Rep.* **2017**, *7*, 17253. [CrossRef]
97. Stumpp, M.; Hu, M.Y.; Melzner, F.; Gutowska, M.A.; Dorey, N.; Himmerkus, N.; Holtmann, W.C.; Dupont, S.T.; Thorndyke, M.C.; Bleich, M. Acidified seawater impacts sea urchin larvae pH regulatory systems relevant for calcification. *Proc. Natl. Acad. Sci. USA* **2012**, *109*, 18192–18197. [CrossRef]
98. Wood, H.L.; Spicer, J.I.; Widdicombe, S. Ocean acidification may increase calcification rates, but at a cost. *Proc. Biol. Sci.* **2008**, *275*, 1767–1773. [CrossRef] [PubMed]
99. Pelletier, G.; Lewis, E.; Wallace, D. CO2SYS.xls: A calculator for the CO2 System in Seawater for Microsoft Excel/VBA. 2007. Available online: https://www.baltex-research.eu/baltic2009/downloads/Lectures/Bernd_Schneider/co2sys_ver14.xls (accessed on 19 January 2022).
100. Hansson, I. A new set of acidity constants for carbonic acid and boric acid in sea water. *Deep Sea Res. Oceanogr. Abstr.* **1973**, *20*, 461–478. [CrossRef]
101. Mehrbach, C.; Culberson, C.H.; Hawley, J.E.; Pytkowicx, R.M. Measurement of the apparent dissociation constants of carbonic acid in seawater at atmospheric pressure. *Limnol. Oceanogr.* **1973**, *18*, 897–907. [CrossRef]
102. Dickson, A.; Millero, F. A comparison of the equilibrium constants for the dissociation of carbonic acid in seawater media. *Deep Sea Res. Part A Oceanogr. Res. Pap.* **1987**, *34*, 1733–1743. [CrossRef]
103. Dickson, A.G. Standard potential of the reaction: AgCl(s) + 1/2H2(g) = Ag(s) + HCl(aq), and the standard acidity constant of the ion HSO4- in synthetic seawater from 273.15 to 318.15 K. *J. Chem. Thermodyn.* **1990**, *22*, 113–127. [CrossRef]
104. Dickson, A.; Riley, J. The estimation of acid dissociation constants in seawater media from potentionmetric titrations with strong base. I. The ionic product of water—Kw. *Mar. Chem.* **1979**, *7*, 89–99. [CrossRef]
105. Uppström, L.R. The boron/chlorinity ratio of deep-sea water from the Pacific Ocean. *Deep Sea Res. Oceanogr. Abstr.* **1974**, *21*, 161–162. [CrossRef]
106. Mucci, A. The solubility of calcite and aragonite in seawater at various salinities, temperatures, and one atmosphere total pressure. *Am. J. Sci.* **1983**, *283*, 780–799. [CrossRef]